Rapid Communications

Equation of state of dense matter in the multimessenger era

Ying Zhou,[1] Lie-Wen Chen,[1,*] and Zhen Zhang[2]

[1]School of Physics and Astronomy and Shanghai Key Laboratory for Particle Physics and Cosmology, Shanghai Jiao Tong University, Shanghai 200240, China

[2]Sino-French Institute of Nuclear Engineering and Technology, Sun Yat-sen University, Zhuhai 519082, China

(Received 1 February 2019; published 3 June 2019)

While the equation of state (EOS) of symmetric nuclear matter (SNM) at suprasaturation densities has been relatively well constrained from heavy-ion collisions, the EOS of high-density neutron-rich matter is still largely uncertain due to the poorly known high-density behavior of the symmetry energy. Using the constraints on the EOS of SNM at suprasaturation densities from heavy-ion collisions together with the data of finite nuclei and the existence of 2 $M_\odot$ neutron stars from electromagnetic observations, we show that the high-density symmetry energy cannot be too soft, which leads to lower bounds on dimensionless tidal deformability of $\Lambda_{1.4} \geq 193$ and radius of $R_{1.4} \geq 11.1$ km for 1.4 $M_\odot$ neutron star. Furthermore, we find that the recent constraint of $\Lambda_{1.4} \leq 580$ from the gravitational wave signal GW170817 detected from the binary neutron star merger by the LIGO and Virgo collaborations rules out too-stiff high-density symmetry energy, leading to an upper limit of $R_{1.4} \leq 13.3$ km. All these terrestrial nuclear experiments and astrophysical observations based on strong, electromagnetic, and gravitational measurements together put stringent constraints on the high-density symmetry energy and the EOS of SNM, pure neutron matter, and neutron star matter.

DOI: 10.1103/PhysRevD.99.121301

I. INTRODUCTION

Dense matter with density comparable to nuclear saturation density n_0 (approximately 0.16 nucleons/ fm^3$\approx$ 2.7×10^{14} g/cm^3) can exist in heavy atomic nuclei and in compact stars or can be produced in heavy-ion collisions. A basic model for understanding such dense matter is the nuclear matter—an ideal static infinite uniform system composed of nucleons (neutrons and protons) with only the strong interaction considered. One fundamental issue in nuclear physics, particle physics, and astrophysics is to explore the equation of state (EOS) of nuclear matter [1–3], conventionally defined as energy (or pressure) vs density. Because of the complicated nonperturbative feature of QCD, it is still a big challenge to determine the nuclear matter EOS from *ab initio* QCD calculations, especially at suprasaturation densities [4]. Therefore, data from terrestrial experiments or astrophysical observations are particularly important to constrain the nuclear matter EOS.

Indeed, the EOS of symmetric nuclear matter (SNM) with an equal fraction of neutrons and protons has been relatively well constrained from around n_0 to about $5n_0$ by analyzing the data on giant monopole resonance of heavy nuclei [5,6] as well as the kaon production [7,8] and collective flow [1] in heavy-ion collisions. On the other hand, the EOS of dense neutron-rich matter, especially at suprasaturation densities, remains largely uncertain due to the poorly known high-density behavior of the isospin-dependent part of nuclear matter EOS, characterized by the symmetry energy $E_{\rm sym}(n)$ (see, e.g., Ref. [9]).

Nuclear data, including those from nuclear structure and heavy-ion collisions, usually have difficulty constraining the high-density $E_{\rm sym}(n)$, although its subsaturation density behavior has been relatively well determined. For example, the nuclear mass can put stringent constraints on $E_{\rm sym}(n)$ around $2/3n_0$ (the averaged density of nuclei) [10], while the electric dipole polarizability is mainly sensitive to the $E_{\rm sym}(n)$ around $1/3n_0$ since isovector giant dipole resonances are essentially related to the neutrons and protons in the nuclear surface [11]. Heavy-ion collisions perhaps are the only way in terrestrial laboratories to produce high-density matter, but the isospin asymmetry is usually small, and thus the current constraints on high-density $E_{\rm sym}(n)$ are strongly model dependent [12–17].

In nature, neutron stars (NSs) provide an ideal site to explore dense matter. The discovery of the currently heaviest neutron star PSR J0348 + 0432 [18] with mass 2.01 ± 0.04 $M_\odot$ actually rules out soft NS matter EOSs, which are not stiff enough against gravitational collapse. The NS mass-radius ($M - R$) relation has been shown to be sensitive to the high-density $E_{\rm sym}(n)$ [19–22] since the averaged density of a NS is about $2.5n_0$ and the NS matter is dominated by neutrons with a small fraction (approximately 10%) of

*Corresponding author.
lwchen@sjtu.edu.cn

protons (and leptons to keep weak equilibrium and charge neutrality). Although the NS mass can be determined precisely, the precise measurement of its radius remains a big challenge [23]. A good probe of the NS radius is the tidal deformability, i.e., the ratio of the induced quadrupole moment of a neutron star to the perturbing tidal field of its companion, and for a NS with mass M, it can be expressed in dimensionless form as [24,25]

$$\Lambda_M = \frac{2}{3} k_2 \left(\frac{c^2 R}{GM}\right)^5, \tag{1}$$

where k_2 is the tidal Love number and R is the NS radius. The inspiraling binary neutron star (BNS) merger, one important source of gravitational waves (GWs) that can be detected by ground-based GW detectors, provides a natural laboratory to extract information on Λ_M. During the BNS inspiral stage before merger, the tidal effects change the phase evolution of the GW waveform compared to that of a binary black hole (BBH) inspiral, and the difference between BNS and BBH inspirals appears from the fifth post-Newtonian order onward with the leading-order contribution proportional to Λ_M [25–27]. The Λ_M can thus be extracted from the GW signal of the BNS inspiral [25,28–30].

On August 17, 2017, the first GW signal GW170817 of BNS merger was observed and localized by the LIGO and Virgo observatories [31], and its electromagnetic (EM) radiation was also detected by many collaborations (see, e.g., Ref. [32]), inaugurating a new era of multimessenger astronomy. Using the GW170817 signal, a large number of studies [33–46] have been performed to constrain the EOS of NS matter or the properties of NSs. The original analysis of GW170817 suggests an upper limit of $\Lambda_{1.4} \leq 800$ [31], and a more recent analysis [47] with some plausible assumptions leads to a stronger constraint of $\Lambda_{1.4} = 190^{+390}_{-120}$.

In this work, for the first time, by using the same model to simultaneously analyze the data based on strong, EM, and gravitational measurements, i.e., the terrestrial data of finite nuclei and heavy-ion collisions, the existence of 2 $M_\odot$ NSs from EM observations, and the upper limit of $\Lambda_{1.4} \leq 580$ from GW170817, we put stringent constraints on the high-density $E_{\rm sym}(n)$ and the EOS of SNM, pure neutron matter (PNM), and NS matter.

II. METHODS

The nuclear matter EOS, defined as the binding energy per nucleon, can be expressed as the parabolic approximation form

$$E(n,\delta) = E_0(n) + E_{\rm sym}(n)\delta^2 + \mathcal{O}(\delta^4), \tag{2}$$

where $n = n_{\rm n} + n_{\rm p}$ is the nucleon number density and $\delta = (n_{\rm n} - n_{\rm p})/n$ is the isospin asymmetry with $n_{\rm p}$ and $n_{\rm n}$ denoting the proton and neutron densities, respectively. $E_0(n) = E(n, \delta = 0)$ is the EOS of SNM, and the symmetry energy is defined by $E_{\rm sym}(n) = \frac{1}{2!}\frac{\partial^2 E(n,\delta)}{\partial \delta^2}|_{\delta=0}$. At the saturation density n_0, the $E_0(n)$ can be expanded in $\chi = (n - n_0)/3n_0$ as $E_0(n) = E_0(n_0) + \frac{1}{2!}K_0\chi^2 + \frac{1}{3!}J_0\chi^3 + \mathcal{O}(\chi^4)$, where K_0 is the incompressibility coefficient and J_0 is the skewness coefficient. The $E_{\rm sym}(n)$ can be expanded at a reference density n_r in terms of the slope parameter $L(n_r)$ and the curvature parameter $K_{\rm sym}(n_r)$ as $E_{\rm sym}(n) = E_{\rm sym}(n_r) + L(n_r)\chi_r + \frac{1}{2!}K_{\rm sym}(n_r)\chi_r^2 + \mathcal{O}(\chi_r^3)$, with $\chi_r = (n - n_r)/(3n_r)$. Conventionally, we have $L \equiv L(n_0)$ and $K_{\rm sym} \equiv K_{\rm sym}(n_0)$.

In this work, we apply the extended Skyrme-Hartree-Fock (eSHF) model [48,49] to three systems, i.e., nuclear matter, finite nuclei, and neutron stars. As emphasized in Ref. [49], the eSHF model includes additional momentum and density-dependent two-body forces to effectively mimic the momentum dependence of the three-body force and can very successfully describe simultaneously the three systems which involve a wide density region and thus is especially suitable for our present motivation. The extended Skyrme interaction is expressed as [48,49]

$$\begin{aligned} v_{i,j} = {} & t_0(1 + x_0 P_\sigma)\delta(\boldsymbol{r}) + \frac{1}{6}t_3(1 + x_3 P_\sigma)n^\alpha(\boldsymbol{R})\delta(\boldsymbol{r}) \\ & + \frac{1}{2}t_1(1 + x_1 P_\sigma)[K'^2\delta(\boldsymbol{r}) + \delta(\boldsymbol{r})K^2] \\ & + t_2(1 + x_2 P_\sigma)\boldsymbol{K}'\cdot\delta(\boldsymbol{r})\boldsymbol{K} + \frac{1}{2}t_4(1 + x_4 P_\sigma) \\ & \times [K'^2\delta(\boldsymbol{r})n(\boldsymbol{R}) + n(\boldsymbol{R})\delta(\boldsymbol{r})K^2] \\ & + t_5(1 + x_5 P_\sigma)\boldsymbol{K}'\cdot n(\boldsymbol{R})\delta(\boldsymbol{r})\boldsymbol{K} \\ & + iW_0(\boldsymbol{\sigma}_i + \boldsymbol{\sigma}_j)\cdot[\boldsymbol{K}'\times\delta(\boldsymbol{r})\boldsymbol{K}], \end{aligned} \tag{3}$$

where the symbols have their conventional meaning [48,49]. The interaction contains 14 independent parameters, i.e., the 13 Skyrme parameters α, $t_0 \sim t_5$, $x_0 \sim x_5$, and the spin-orbit coupling constant W_0. Instead of directly using the 13 Skyrme parameters, we express them explicitly in terms of the following 13 macroscopic quantities (pseudoparameters) [49]: n_0, $E_0(n_0)$, K_0, J_0, $E_{\rm sym}(n_r)$, $L(n_r)$, $K_{\rm sym}(n_r)$, the isoscalar effective mass $m^*_{s,0}$, the isovector effective mass $m^*_{v,0}$, the gradient coefficient G_S, the symmetry-gradient coefficient G_V, the cross gradient coefficient G_{SV}, and the Landau parameter G'_0 of SNM in the spin-isospin channel. The higher-order parameters J_0 and $K_{\rm sym}$ generally have small influence on the properties of finite nuclei but are critical for the high-density neutron-rich matter EOS and NS properties. In addition, at the subsaturation density $n_c = 0.11n_0/0.16$, the $E_{\rm sym}(n_c)$ has been precisely constrained to be $E_{\rm sym}(n_c) = 26.65 \pm 0.2$ MeV [10] by analyzing the binding energy difference of heavy isotope pairs, and $L(n_c) = 47.3 \pm 7.8$ MeV [50] is extracted from the electric dipole polarizability of ^{208}Pb. Therefore, here, we fix J_0 and $K_{\rm sym}$ at various values with

$E_{\rm sym}(n_c) = 26.65$ MeV and $L(n_c) = 47.3$ MeV, and the other ten parameters are obtained by fitting the data of finite nuclei by minimizing the weighted sum of the squared deviations between the theoretical predictions and the experimental data, i.e., $\chi^2(\boldsymbol{p}) = \sum_{i=1}^{N} \left(\frac{\mathcal{O}_i^{\rm th}(\boldsymbol{p}) - \mathcal{O}_i^{\rm exp}}{\Delta\mathcal{O}_i}\right)^2$, where the $\boldsymbol{p} = (p_1, \ldots, p_z)$ define the z-dimensional model space; $\mathcal{O}_i^{\rm (th)}$ and $\mathcal{O}_i^{\rm (exp)}$ are the theoretical predictions and the corresponding experimental values of observables, respectively; and $\Delta\mathcal{O}_i$ is the adopted error used to balance the relative weights of the various types of observables. We note here that varying $L(n_c)$ within $L(n_c) = 47.3 \pm 7.8$ MeV mainly influences the values of G_S, G_V, and G_{SV}, which are irrelevant to the nuclear matter EOS, while the parameters n_0, $E_0(n_0)$, and K_0 characterizing the nuclear matter EOS remain almost unchanged.

In the fitting, we consider the following experimental data of spherical even-even nuclei: (i) the binding energies $E_{\rm B}$ of ^{16}O, ^{40,48}Ca, ^{56,68}Ni, ^{88}Sr, ^{90}Zr, ^{100,116,132}Sn, ^{144}Sm, and ^{208}Pb [51]; (ii) the charge rms radii $r_{\rm c}$ of ^{16}O, ^{40,48}Ca, ^{56}Ni, ^{88}Sr, ^{90}Zr, ^{116}Sn, ^{144}Sm, and ^{208}Pb [52–54]; (iii) the isoscalar giant monopole resonance energies $E_{\rm GMR}$ of ^{90}Zr, ^{116}Sn, ^{144}Sm, and ^{208}Pb [5]; and (iv) the spin-orbit energy level splittings $\epsilon_{\rm ls}^A$ for neutron $1p_{1/2} - 1p_{3/2}$ and proton $1p_{1/2} - 1p_{3/2}$ in ^{16}O and the proton $2d_{3/2} - 2d_{5/2}$, neutron $3p_{1/2} - 3p_{3/2}$, and neutron $2f_{5/2} - 2f_{7/2}$ in ^{208}Pb [55]. To balance the χ^2 from each sort of experimental data (see, e.g., Ref. [49]), we assign the errors of 1.0 MeV and 0.01 fm to the $E_{\rm B}$ and $r_{\rm c}$, respectively. In particular, for the $E_{\rm GMR}$, we use the experimental error multiplied by 3.5 to also consider the impact of the experimental error, while for the $\epsilon_{\rm ls}^A$, a 10% relative error is employed.

For NSs, we consider here the conventional NS model, which includes only nucleons, electrons, and possible muons ($npe\mu$), and the NS is assumed to contain a core, inner crust, and outer crust. For the core, the EOS of β-stable and electrically neutral $npe\mu$ matter is obtained from the eSHF model. For the inner crust in the density region between $n_{\rm out}$ and $n_{\rm t}$, the EOS is constructed by interpolating with $P = a + b\mathcal{E}^{4/3}$ [56], where P is pressure and $\mathcal{E}$ is energy density. The density $n_{\rm out}$ separating the inner and the outer crusts is taken to be 2.46×10^{-4} fm^{-3}, while the core-crust transition density $n_{\rm t}$ is evaluated self-consistently by a dynamical approach [57]. For the outer crust, we use the well-known Baym-Pethick-Sutherland EOS in the density region of 6.93×10^{-13} fm$^{-3} < n < n_{\rm out}$ and the Feynman-Metropolis-Teller EOS for 4.73×10^{-15} fm$^{-3} < n < 6.93 \times 10^{-13}$ fm^{-3} [58,59]. It should be noted that all the extended Skyrme interactions used in the following NS calculations satisfy the causality condition $dP/d\mathcal{E} < 1$.

III. RESULTS AND DISCUSSIONS

Shown in Fig. 1 is the pressure vs the density for SNM within eSHF in various extended Skyrme parameter sets

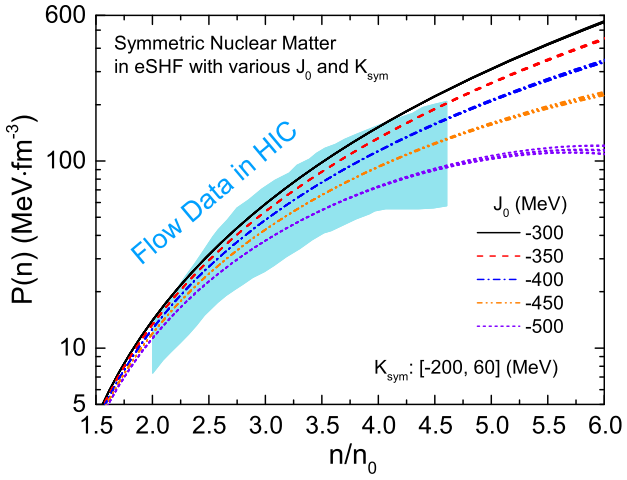

FIG. 1. Pressure vs density for SNM within eSHF in various extended Skyrme interactions with J_0 and $K_{\rm sym}$ fixed at various values. The constraint from collective flow data in heavy-ion collisions [1] is included for comparison.

with J_0 fixed at $(-300, -350, -400, -450, -500)$ MeV and $K_{\rm sym}$ in the range of $(-200, 60)$ MeV. Also included in the figure is the constraint from collective flow data in heavy-ion collisions [1]. For all the parameter sets with fixed J_0 and $K_{\rm sym}$, as expected, the total chi-square $\chi^2_{\rm tot}$ falls in the range of $24.45 < \chi^2_{\rm tot} < 36.24$, and the mean χ^2 of each sort of experimental data (i.e., $\chi^2_{E_{\rm B}}/12$, $\chi^2_{r_{\rm c}}/9$, $\chi^2_{E_{\rm GMR}}/4$, and $\chi^2_{\epsilon_{\rm ls}^A}/5$) is approximately equal to 1. The small variation of $\chi^2_{\rm tot}$ suggests that the higher-order parameters J_0 and $K_{\rm sym}$ indeed have small influence on the properties of finite nuclei. In addition, the pressure of SNM exhibits negligible dependence on the $K_{\rm sym}$, especially for $J_0 > -500$ MeV. One sees that the pressure of SNM becomes stiffer as the J_0 increases, and $J_0 = -300$ MeV predicts a too-stiff SNM EOS that violates the flow data. A detailed study indicates an upper limit at $J_0^{\rm up} = -342$ MeV.

Using the same parameter sets as used in Fig. 1, we show in Fig. 2 the NS maximum mass $M_{\rm max}$ vs $K_{\rm sym}$. One sees the $M_{\rm max}$ increases sensitively with increasing J_0 for a fixed $K_{\rm sym}$. The $K_{\rm sym}$ has small influence on the $M_{\rm max}$ when $K_{\rm sym}$ is greater than about -100 MeV, but for a fixed J_0, the $M_{\rm max}$ is drastically reduced with decreasing $K_{\rm sym}$ for $K_{\rm sym} \lesssim -100$ MeV. This behavior is due to the fact that a larger $K_{\rm sym}$ leads to a stiffer high-density symmetry energy and thus smaller isospin asymmetry in high-density NS matter. The smaller isospin asymmetry in turn suppresses the sensitivity of $M_{\rm max}$ to $K_{\rm sym}$, as the $M_{\rm max}$ is mainly determined by the EOS of high-density NS matter. In particular, for sufficiently large $K_{\rm sym}$ (e.g., $\gtrsim -100$ MeV), the NS matter can become almost isospin symmetric at high densities, and the NS maximum mass is therefore mainly sensitive to J_0, which dominates the high-density behavior of symmetric nuclear matter. Since the

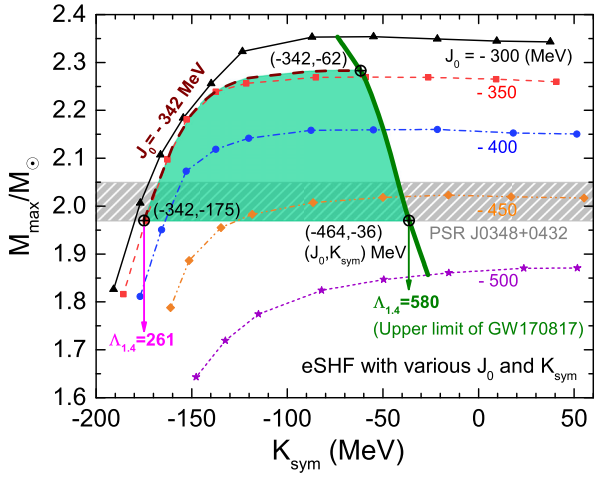

FIG. 2. NS maximum mass $M_{\max}$ vs $K_{\rm sym}$ within eSHF in various extended Skyrme interactions with J_0 and $K_{\rm sym}$ fixed at various values. See the text for details.

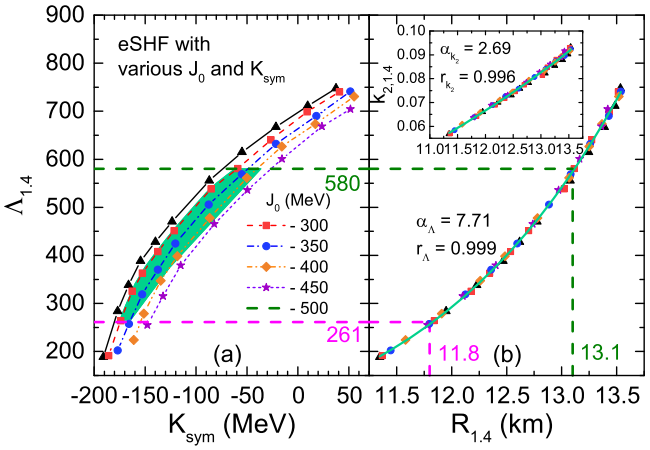

FIG. 3. $\Lambda_{1.4}$ vs $K_{\rm sym}$ (a) and $\Lambda_{1.4}$ vs $R_{1.4}$ (b) within eSHF using the same extended Skyrme parameter sets as used in Fig. 2. The results for $k_{2,1.4}$ vs $R_{1.4}$ are included in the inset of panel (b). See the text for details.

flow data in heavy-ion collisions require $J_0 \leq -342$ MeV, the parameter sets with $J_0 = -342$ MeV generally predict he largest values of $M_{\max}$, and the corresponding results are also included Fig. 2. For $J_0 = -342$ MeV, it is seen that when $K_{\rm sym}$ is smaller than -175 MeV the predicted $M_{\max}$ starts violating the mass lower limit (i.e., 1.97 $M_\odot$) of the heaviest NS PSR J0348 + 0432 [18] observed so far (its mass 2.01 ± 0.04 $M_\odot$ is shown as a shaded band in Fig. 2), leading to a lower limit at $K_{\rm sym}^{\rm low} = -175$ MeV. For a fixed J_0, we find that the $\Lambda_{1.4}$ rapidly increases with increasing $K_{\rm sym}$. For a fixed $K_{\rm sym}$, the $\Lambda_{1.4}$ also increases with J_0 but is much weaker than that with $K_{\rm sym}$. Our results indicate that the data of finite nuclei, the flow data in heavy-ion collisions, and the existence of 2 $M_\odot$ NS together give the limit of $K_{\rm sym} \geq -175$ MeV, leading to a lower limit of $\Lambda_{1.4}^{\rm low} = 261$.

The above analyses mean the $E_{\rm sym}(n)$ cannot be too soft. When the $K_{\rm sym}$ increases, the $E_{\rm sym}(n)$ becomes stiffer, and the $\Lambda_{1.4}$ increases accordingly. The most recent limit of $\Lambda_{1.4} \leq 580$ [47] thus can put an upper limit for $K_{\rm sym}$ for each J_0 as indicated Fig. 2. The limit of $\Lambda_{1.4} \leq 580$ together with the data of finite nuclei, the flow data in heavy-ion collisions, and the existence of 2 $M_\odot$ NS thus give an allowed region for the higher-order parameters J_0 and $K_{\rm sym}$, as shown by the green region in Fig. 2, which leads to -464 MeV $\leq J_0 \leq -342$ MeV and -175 MeV $\leq K_{\rm sym} \leq -36$ MeV. Moreover, the largest NS mass is determined to be 2.28 $M_\odot$ at $(J_0, K_{\rm sym}) = (-342, -62)$ MeV as indicated in Fig. 2.

Shown in Fig. 3(a) is $\Lambda_{1.4}$ vs $K_{\rm sym}$ within eSHF using the same parameter sets as used in Fig. 2. The corresponding results for $\Lambda_{1.4}$ vs $R_{1.4}$ are shown in Fig. 3(b), and the inset in Fig. 3(b) displays the results for $k_{2,1.4}$ vs $R_{1.4}$. The allowed region for J_0 and $K_{\rm sym}$ is also included in Fig. 3(a). As already mentioned, one indeed sees that $\Lambda_{1.4}$ is sensitive to $K_{\rm sym}$ but is less affected by the J_0. From Fig. 3(b) and the inset, one sees both $\Lambda_{1.4}$ and $k_{2,1.4}$ exhibit very strong correlation with $R_{1.4}$, and they can be nicely fitted by the formulas $\Lambda_{1.4} = a_\Lambda R_{1.4}^{\alpha_\Lambda}$ and $k_{2,1.4} = a_{k_2} R_{1.4}^{\alpha_{k_2}}$, respectively, with $a_\Lambda = (1.41 \pm 0.14) \times 10^{-6}$, $\alpha_\Lambda = 7.71 \pm 0.04$, $a_{k_2} = (8.25 \pm 0.58) \times 10^{-5}$, and $\alpha_{k_2} = 2.69 \pm 0.03$. The correlation coefficient is $r_\Lambda = 0.999$ for $\Lambda_{1.4} = a_\Lambda R_{1.4}^{\alpha_\Lambda}$ and $r_{k_2} = 0.996$ for $k_{2,1.4} = a_{k_2} R_{1.4}^{\alpha_{k_2}}$. These relations together with $261 \leq \Lambda_{1.4} \leq 580$ lead to the stringent constraints of $R_{1.4} \in [11.8, 13.1]$ km and $k_{2,1.4} \in [0.064, 0.085]$.

According to the allowed parameter space for J_0 and $K_{\rm sym}$ as shown in Fig. 2, we can determine the EOS of dense matter. The obtained results for $E_{\rm sym}(n)$ are shown in Fig. 4(a), and the pressure vs density for SNM, PNM, and NS matter is exhibited in Figs. 4(b), 4(c), and 4(d), respectively. Also included in Fig. 4(a) are the constraints at subsaturation densities from midperipheral heavy-ion collisions of Sn isotopes [60], the isobaric analog states (IASs) and combining the neutron skin data (IAS + NSkin) [61], and the electric dipole polarizability (α_D) in ^{208}Pb [11]. In addition, the constraints on pressure for SNM from flow data in heavy-ion collisions [1] and that for NS matter from GW170817 [47] are also included in Figs. 4(b) and 4(d), respectively. Furthermore, we include the corresponding results with $L(n_c) = 55.1$ MeV and 39.5 MeV to display the uncertainty due to the $L(n_c)$ (i.e., $L(n_c) = 47.3 \pm 7.8$ MeV [50]). One sees that our results are consistent with the existing constraints but with much higher precision due to the simultaneous consideration of the data of finite nuclei, the flow data in heavy-ion collisions, the observed heaviest NS, and the GW170817 signal. We would like to point out that the high-density $E_{\rm sym}(n)$ still has large uncertainty and it could be negative at high densities, which would cause isospin instability and thus the presence of a PNM core in NSs.

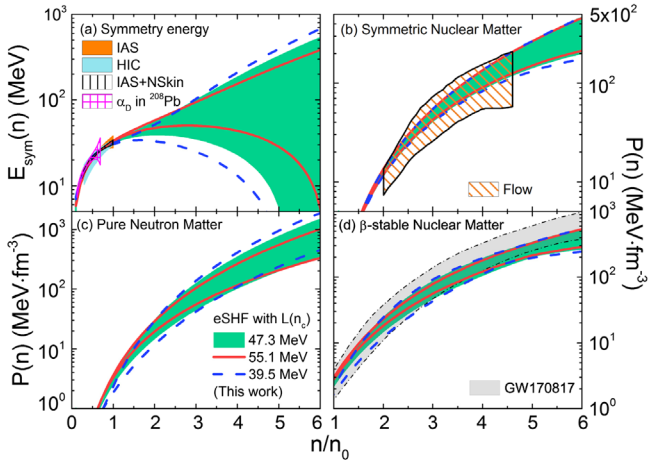

FIG. 4. Density dependence of the symmetry energy (a) and pressure for SNM (b), PNM (c), and neutron star matter (d). See the text for details.

Furthermore, our results indicate that the $L(n_c) = 39.5$ MeV gives lower limits of $K_{\rm sym}$, $\Lambda_{1.4}$, J_0 as $K_{\rm sym}^{\rm low} = -203$ MeV, $\Lambda_{1.4}^{\rm low} = 193$, $J_0^{\rm low} = -475$ MeV and the maximum NS mass of $M_{\rm max} = 2.30 M_\odot$, while $L(n_c) = 55.1$ MeV gives $K_{\rm sym}^{\rm low} = -138$ MeV, $\Lambda_{1.4}^{\rm low} = 380$, $J_0^{\rm low} = -455$ MeV and $M_{\rm max} = 2.26 M_\odot$. In addition, the $E_{\rm sym}(2n_0)$ is found to be [46.9, 57.6] MeV, [39.4, 54.5] MeV, and [33.0, 51.3] MeV for $L(n_c) = 39.5$ MeV, 47.3 MeV, and 51.1 MeV, respectively. Using $L(n_c) = 47.3 \pm 7.8$ MeV, therefore, we obtain $J_0 \in [-464^{+9}_{-11}, -342]$ MeV, $K_{\rm sym} \in [-175^{+37}_{-28}, -36 \mp 2]$ MeV, $E_{\rm sym}(2n_0) \in [39.4^{-6.4}_{+7.5}, 54.5^{-3.2}_{+3.1}]$ MeV, $\Lambda_{1.4} \in [261^{+119}_{-68}, 580]$, $R_{1.4} \in [11.8^{+0.8}_{-0.7}, 13.1 \pm 0.2]$ km, and $M_{\rm max} = 2.28 \mp 0.02\ M_\odot$.

For the higher-order parameters J_0 and $K_{\rm sym}$, the $J_0 \in [-464^{+9}_{-11}, -342]$ MeV gives the strongest constraint compared to the existing ones [62], and the $K_{\rm sym} \in [-175^{+37}_{-28}, -36 \mp 2]$ MeV is also consistent with those extracted from the symmetry energy systematics with some correlations [46,63–65] or from heavy-ion collisions [17]. Moreover, the $E_{\rm sym}(2n_0) \in [39.4^{-6.4}_{+7.5}, 54.5^{-3.2}_{+3.1}]$ MeV is in good agreement with those extracted from the symmetry energy systematics [64], heavy-ion collisions [16], and the recent analyses on the NS observation and the GW170817 signal [38,39]. As for the NS properties, the $\Lambda_{1.4}^{\rm low} = 261^{+119}_{-68}$ agrees with the constraints from analyzing the GW170817 signal [40,41] or its EM signals [42,43], the $R_{1.4} \in [11.8^{+0.8}_{-0.7}, 13.1 \pm 0.2]$ km agrees with those from analyzing the GW170817 [40,41,46], and the $M_{\rm max} = 2.28 \mp 0.02\ M_\odot$ is consistent with the results from analyzing GW170817 [44,45].

Although the polytropic form of $P = a + b\mathcal{E}^{4/3}$ has been extensively used to approximate the EOS of the NS inner crust [20,49,56,57], where the nuclear pasta may exist, the sensitivity of our results to the choice of polytropic index needs to be studied. For an example, based on the EOS with $J_0 = -342$ MeV and $K_{\rm sym} = -175$ MeV, which gives $M_{\rm max} = 1.97\ M_\odot$, we obtain $\Lambda_{1.4} = 261.76(260.86, 260.50)$, $R_{1.4} = 12.52(11.82, 11.55)$ km and $k_{2,1.4} = 0.048(0.064, 0.071)$ with the polytropic index $1(4/3, 5/3)$. These results indicate that the increase of the polytropic index leads to a considerable increase of the $k_{2,1.4}$, small reduction (less than 10%) of $R_{1.4}$, and a negligible decrease of $\Lambda_{1.4}$, suggesting the choice of the polytropic index has negligible effects on $\Lambda_{1.4}$.

IV. SUMMARY

Using the eSHF model to simultaneously analyze the data from terrestrial nuclear experiments and astrophysical observations based on strong, EM, and gravitational measurements, we have put stringent constraints on the high-density $E_{\rm sym}(n)$ and the pressure of SNM, PNM, and NS matter. We have found that the nuclear data and the existence of $2\ M_\odot$ NS rule out too-soft high-density $E_{\rm sym}(n)$, leading to lower limits of $\Lambda_{1.4} \geq 193$ and $R_{1.4} \geq 11.1$ km. Further combining the upper limit of $\Lambda_{1.4} \leq 580$ from GW170817 excludes too-stiff high-density $E_{\rm sym}(n)$, leading to an upper limit of $R_{1.4} \leq 13.3$ km. Using $L(n_c) = 47.3 \pm 7.8$ MeV, we have obtained $J_0 \in [-464^{+9}_{-11}, -342]$ MeV, $K_{\rm sym} \in [-175^{+37}_{-28}, -36 \mp 2]$ MeV, $E_{\rm sym}(2n_0) \in [39.4^{-6.4}_{+7.5}, 54.5^{-3.2}_{+3.1}]$ MeV, and $M_{\rm max} = 2.28 \mp 0.02\ M_\odot$. In the future, a more precise limit on $L(n_c)$, the possible discovery of heavier NS, and a tighter bound on $\Lambda_{1.4}$ from BNS merger will put stronger constraints on the high-density $E_{\rm sym}(n)$ and thus the EOS of dense neutron-rich matter.

ACKNOWLEDGMENTS

The authors thank Tanja Hinderer, Ang Li, Bao-An Li, and Jorge Piekarewicz for helpful discussions. This work was supported in part by the National Natural Science Foundation of China under Grant No. 11625521; the Major State Basic Research Development Program (973 Program) in China under Contract No. 2015CB856904; the Program for Professor of Special Appointment (Eastern Scholar) at Shanghai Institutions of Higher Learning, Key Laboratory for Particle Physics, Astrophysics and Cosmology, Ministry of Education, China; and the Science and Technology Commission of Shanghai Municipality (Grant No. 11DZ2260700).

[1] P. Danielewicz, R. Lacey, and W. G. Lynch, Science **298**, 1592 (2002).
[2] J. M. Lattimer and M. Prakash, Science **304**, 536 (2004).
[3] M. Oertel, M. Hempel, T. Klahn, and S. Typel, Rev. Mod. Phys. **89**, 015007 (2017).
[4] N. Brambilla *et al.*, Eur. Phys. J. C **74**, 2981 (2014).
[5] D. H. Youngblood, H. L. Clark, and Y.-W. Lui, Phys. Rev. Lett. **82**, 691 (1999).
[6] U. Garg and G. Colò, Prog. Part. Nucl. Phys. **101**, 55 (2018).
[7] J. Aichelin and C. M. Ko, Phys. Rev. Lett. **55**, 2661 (1985).
[8] C. Fuchs, Prog. Part. Nucl. Phys. **56**, 1 (2006).
[9] B. A. Li, L. W. Chen, and C. M. Ko, Phys. Rep. **464**, 113 (2008).
[10] Z. Zhang and L. W. Chen, Phys. Lett. B **726**, 234 (2013).
[11] Z. Zhang and L. W. Chen, Phys. Rev. C **92**, 031301(R) (2015).
[12] Z. Xiao, B. A. Li, L. W. Chen, G. C. Yong, and M. Zhang, Phys. Rev. Lett. **102**, 062502 (2009).
[13] Z. Q. Feng and G. M. Jin, Phys. Lett. B **683**, 140 (2010).
[14] P. Russotto *et al.*, Phys. Lett. B **697**, 471 (2011).
[15] M. D. Cozma, Y. Leifels, W. Trautmann, Q. Li, and P. Russotto, Phys. Rev. C **88**, 044912 (2013).
[16] P. Russotto *et al.*, Phys. Rev. C **94**, 034608 (2016).
[17] M. D. Cozma, Eur. Phys. J. A **54**, 40 (2018).
[18] J. Antoniadis *et al.*, Science **340**, 1233232 (2013).
[19] L. Lindblom, Astrophys. J. **398**, 569 (1992).
[20] J. M. Lattimer and M. Parakash, Astrophys. J. **550**, 426 (2001).
[21] F. Özel, G. Baym, and T. Guver, Phys. Rev. D **82**, 101301 (R) (2010).
[22] A. W. Steiner, J. M. Lattimer, and E. F. Brown, Astrophys. J. **722**, 33 (2010).
[23] F. Özel and P. Freire, Annu. Rev. Astron. Astrophys. **54**, 401 (2016).
[24] T. Hinderer, Astrophys. J. **677**, 1216 (2008).
[25] É. É. Flanagan and T. Hinderer, Phys. Rev. D **77**, 021502(R) (2008).
[26] T. Damour and A. Nagar, Phys. Rev. D **80**, 084035 (2009).
[27] S. E. Gralla, Classical Quantum Gravity **35**, 085002 (2018).
[28] T. Hinderer, B. D. Lackey, R. N. Lang, and J. S. Read, Phys. Rev. D **81**, 123016 (2010).
[29] J. Vines, É. É. Flanagan, and T. Hinderer, Phys. Rev. D **83**, 084051 (2011).
[30] T. Damour, A. Nagar, and L. Villain, Phys. Rev. D **85**, 123007 (2012).
[31] B. P. Abbott *et al.*, Phys. Rev. Lett. **119**, 161101 (2017).
[32] B. P. Abbott *et al.*, Astrophys. J. Lett. **848**, L12 (2017).
[33] B. Margalit and B. D. Metzger, Astrophys. J. Lett. **850**, L19 (2017).
[34] A. Bauswein, O. Just, H.-T. Janka, and N. Stergioulas, Astrophys. J. Lett. **850**, L34 (2017).
[35] E.-P. Zhou, X. Zhou, and A. Li, Phys. Rev. D **97**, 083015 (2018).
[36] F. J. Fattoyev, J. Piekarewicz, and C. J. Horowitz, Phys. Rev. Lett. **120**, 172702 (2018).
[37] S. De, D. Finstad, J. M. Lattimer, D. A. Brown, E. Berger, and C. M. Biwer, Phys. Rev. Lett. **121**, 091102 (2018).
[38] N. B. Zhang, B. A. Li, and J. Xu, Astrophys. J. **859**, 90 (2018).
[39] N. B. Zhang and B. A. Li, Eur. Phys. J. A **55**, 39 (2019).
[40] E. Annala, T. Gorda, A. Kurkela, and A. Vuorinen, Phys. Rev. Lett. **120**, 172703 (2018).
[41] E. R. Most, L. R. Weih, L. Rezzolla, and J. Schaffner-Bielich, Phys. Rev. Lett. **120**, 261103 (2018).
[42] D. Radice, A. Perego, F. Zappa, and S. Bernuzzi, Astrophys. J. Lett. **852**, L29 (2018).
[43] M. W. Coughlin *et al.*, arXiv:1805.09371.
[44] L. Rezzolla, E. R. Most, and L. R. Weih, Astrophys. J. Lett. **852**, L25 (2018).
[45] M. Ruiz, S. L. Shapiro, and A. Tsokaros, Phys. Rev. D **97**, 021501(R) (2018).
[46] T. Malik, N. Alam, M. Fortin, C. Providência, B. K. Agrawal, T. K. Jha, B. Kumar, and S. K. Patra, Phys. Rev. C **98**, 035804 (2018).
[47] B. P. Abbott *et al.*, Phys. Rev. Lett. **121**, 161101 (2018).
[48] N. Chamel, S. Goriely, and J. M. Pearson, Phys. Rev. C **80**, 065804 (2009).
[49] Z. Zhang and L. W. Chen, Phys. Rev. C **94**, 064326 (2016).
[50] Z. Zhang and L. W. Chen, Phys. Rev. C **90**, 064317 (2014).
[51] M. Wang, G. Audi, F. G. Kondev, W. J. Huang, S. Naimi, and X. Xu, Chin. Phys. C **41**, 030003 (2017).
[52] I. Angeli and K. P. Marinova, At. Data Nucl. Data Tables **99**, 69 (2013).
[53] G. Fricke, C. Bernhardt, K. Heilig, L. A. Schaller, L. Schellenberg, E. B. Shera, and C. W. Dejager, At. Data Nucl. Data Tables **60**, 177 (1995).
[54] F. Le Blanc *et al.*, Phys. Rev. C **72**, 034305 (2005).
[55] D. Vautherin and D. M. Brink, Phys. Rev. C **5**, 626 (1972).
[56] J. Carrier, C. J. Horowitz, and J. Piekarewicz, Astrophys. J. **593**, 463 (2003).
[57] J. Xu, L. W. Chen, B. A. Li, and H. R. Ma, Astrophys. J. **697**, 1549 (2009).
[58] G. Baym, C. Pethick, and P. Sutherland, Astrophys. J. **170**, 299 (1971).
[59] K. Iida and K. Sato, Astrophys. J. **477**, 294 (1997).
[60] M. B. Tsang, Y. Zhang, P. Danielewicz, M. Famiano, Z. Li, W. G. Lynch, and A. W. Steiner, Phys. Rev. Lett. **102**, 122701 (2009).
[61] P. Danielewicz and J. Lee, Nucl. Phys. **A922**, 1 (2014).
[62] B. J. Cai and L. W. Chen, J. Nucl. Sci. Technol. **28**, 185 (2017).
[63] L. W. Chen, Sci. China Phys. Mech. Astron. **54**, s124 (2011).
[64] L. W. Chen, EPJ Web Conf. **88**, 00017 (2015).
[65] C. Mondal, B. K. Agrawal, J. N. De, S. K. Samaddar, M. Centelles, and X. Viñas, Phys. Rev. C **96**, 021302(R) (2017).